



Statistical Analysis of Simulated Spaceborne Thermodynamics Lidar Measurements in the Planetary Boundary Layer

David N. Whiteman^{1*}, Paolo Di Girolamo², Andreas Behrendt³, Volker Wulfmeyer³ and Noemi Franco²

¹Howard University, Washington, DC, United States, ²University of Basilicata, Potenza, Italy, ³University of Hohenheim, Stuttgart, Germany

OPEN ACCESS

Edited by:

Daniel Perez Ramirez,
University of Granada, Spain

Reviewed by:

Amin Nehrir,
National Aeronautics and Space
Administration, United States
Igor Veselovskii,
Prokhorov General Physics Institute
(RAS), Russia

*Correspondence:

David N. Whiteman
dnwhiteman@gmail.com

Specialty section:

This article was submitted to
Lidar Sensing,
a section of the journal
Frontiers in Remote Sensing

Received: 05 November 2021

Accepted: 14 February 2022

Published: 14 March 2022

Citation:

Whiteman DN, Di Girolamo P,
Behrendt A, Wulfmeyer V and
Franco N (2022) Statistical Analysis of
Simulated Spaceborne
Thermodynamics Lidar Measurements
in the Planetary Boundary Layer.
Front. Remote Sens. 3:810032.
doi: 10.3389/frsen.2022.810032

The performance of a spaceborne Raman lidar offering measurements of water vapor, temperature, aerosol backscatter and extinction is assessed statistically by use of a lidar simulator and a global model to provide inputs for simulation. The candidate thermodynamics lidar system is envisioned to make use of a sun-synchronous, dawn/dusk orbit. Cloud-free atmospheric profiles simulated by the NASA/GSFC GEOS model for the orbit of the CALIPSO satellite on 15 July 2009 were used as input to a previously validated lidar simulator where GEOS profiles that satisfy the solar zenith angle restrictions of the dawn/dusk orbit, and are located within the Planetary Boundary Layer as defined by the GEOS model, were selected for the statistical analysis. To assess the performance of the simulated thermodynamics lidar system, measurement goals were established by considering the WMO Observing Systems Capability Analysis and Review (OSCAR) requirements for Numerical Weather Prediction. The efforts of Di Girolamo et al., 2018 established the theoretical basis for the current work and discussed many of the technological considerations for a spaceborne thermodynamics lidar. The work presented here was performed during 2017–2018 under the auspices of the NASA/GSFC Planetary Boundary Layer Science Task Group and expanded on previous efforts by considerably increasing the statistical robustness of the performance simulations and extending the statistics to include those of aerosol backscatter and extinction measurements. Further work that is currently being conducted includes Observing Systems Simulation Experiments to assess the impact of a thermodynamics lidar on global forecast improvement.

Keywords: lidar, spaceborne, thermodynamic profiles, Raman, weather prediction

1 INTRODUCTION

The National Academy of Science (NAS) in the 2018 Decadal Survey (NAS, National Academies of Sciences, Engineering, and Medicine, 2018) identified the Planetary Boundary Layer (PBL) as a key targeted observable and specified lidar as one of the prime technologies for measuring it. There are many reasons for the identified high importance of the PBL within the Decadal Survey. Accurate, high spatial and temporal resolution observations in the PBL of temperature and water vapor,

referred to as thermodynamic profiles, are essential for improving weather forecasting (Crook, 1996; Dierer et al., 2009) and model re-analysis (Bengtsson et al., 2004). Furthermore, these measurements are also important for understanding land-surface interactions and thus parameterizations of those processes and others in regional climate models (Warrach-Sagi et al., 2013; Kotlarski et al., 2014). Wulfmeyer et al., 2015 demonstrated that global scale measurements of thermodynamics profiles within the PBL would have a significant impact on our understanding of the Earth's systems. In response to the NAS findings in the Decadal Survey and in support of European Space Agency initiatives, Di Girolamo et al., 2018 (DiG2018) simulated the measurement capability of a spaceborne thermodynamics lidar utilizing a sun-synchronous dawn/dusk orbit. They studied the performance of the lidar system using US Standard, Tropical, mid-latitude Winter and Summer atmospheres and considered attenuation by clouds. Here we use the NASA/GSFC GEOS model to provide a large number of cloud-free input profiles permitting a statistical analysis of the measurement capability of the thermodynamics lidar system, first studied in DiG2018, within the PBL.

The work reported here occurred during the period 2017–2018 under the auspices of the NASA/GSFC PBL Science Task Group. It is part of an on-going effort, led by the Universities of Basilicata and Hohenheim, focused on determining the utility of spaceborne thermodynamics lidar in improving short term weather forecasting and other predictive parameters. The goal of the overall activity is to use simulated thermodynamics lidar profiling as demonstrated here in Observation Systems Simulation Experiments (OSSE) to assess the impact of the spaceborne lidar system.

The paper is structured as follows. In part 2 we review the methods, pertinent equations and datasets used in the study. In part 3 we provide visual displays of the performance of the spaceborne lidar for measuring temperature, water vapor and aerosols under both day and night, cloud-free, conditions. Then a selection of profiles is made consistent with a dawn/dusk orbit. Using that orbit, the performance of the lidar system within the PBL is analyzed statistically. Part 4 concludes the paper with a discussion of the results here and looks toward the additional work involving OSSEs that fully considers the influence of clouds and is currently in progress.

2 METHODS AND TECHNIQUES

Raman lidar has been used for several decades for a wide variety of studies including that of water vapor profiling in the lower atmosphere (Melfi and Whiteman, 1985, Goldsmith et al., 1998; Whiteman, 2003a; Whiteman, 2003b), temperature profiling in the convective boundary layer (Behrendt et al., 2015), aerosol backscatter and extinction for studying aerosol hygroscopic growth (Ferrare et al., 1998a; Ferrare et al., 1998b; Veselovskii et al., 2009). The lidar technique makes use of a laser transmitter, telescope receiver, wavelength selection optics and sophisticated data acquisition electronics to acquire profiles of atmospheric constituents with high temporal and spatial resolution and has

been extensively discussed previously (e.g., Weitkamp, 2005). The Raman lidar makes use of an inelastic scattering process, first discovered by C. V. Raman and K. S. Krishnan in 1928 (Raman, 1928; Raman and Krishnan, 1928), that exploits molecular vibrational or rotational transitions and spectroscopic techniques in order to identify different atmospheric molecules such as water vapor, nitrogen, oxygen, carbon dioxide, etc.

Much has been written previously about the use of Raman lidar for a wide variety of atmospheric studies so we will refer readers to the references cited above for further background and the equations that give the lidar signal as a function of range. For the purposes of the lidar simulations performed here we will briefly detail the important equations to illustrate which quantities must be simulated in order to assess the measurement performance of the lidar system. The Raman lidar as studied here collects four lidar signals: the water vapor vibrational Raman signal, $P_{H_2O}(z)$, two rotational Raman signals from high- and low-quantum number transitions, $P_{LoJ}(z)$ and $P_{HiJ}(z)$, and the direct backscatter signal at λ_0 , $P_{\lambda_0}(z)$. The fundamental equations for the various P_X terms can be found in the references listed below. One point to note is that the temperature dependence of Raman water vapor scattering (Sherlock et al., 1999, Whiteman, 2003a; Whiteman, 2003b) has not been accounted for in the P_X equations used here since the focus was on determining random uncertainty budgets which are dominated by the Poisson statistics relating to the measurement process and not by the primarily systematic effects introduced by the temperature dependence. Correction techniques for these temperature dependent effects are relatively straightforward and would need to be included in any real space mission but excluding them here does not influence the results of the statistical analysis.

2.1 Calculation of Temperature, Water Vapor Mixing Ratio, Aerosol Backscatter and Extinction

The direct calculation of atmospheric temperature is obtained from the rotational Raman backscattered signals through the expression (Behrendt and Reichardt, 2000):

$$T(z) = \frac{\alpha}{\ln[Q(z) - \beta]} \quad (1)$$

where $Q(z) = P_{HiJ}(z)/P_{LoJ}(z)$ and $P_{LoJ}(z)$ and $P_{HiJ}(z)$ are the low (*LoJ*) and high (*HiJ*) quantum number rotational Raman backscatter signals at wavelengths λ_{LoJ} and λ_{HiJ} , respectively, received from altitude z in the anti-Stokes branch of the rotational Raman spectrum, and α and β are two calibration constants. The spectral locations of λ_{LoJ} and λ_{HiJ} were identified through a sensitivity analysis that accounted for various atmospheric and instrumental parameters such as the signal-to-background ratio, the filter bandwidths and filter shapes, and the temperature range of interest (Hammann and Behrendt, 2015). For the present system, λ_{LoJ} and λ_{HiJ} were identified with the purpose of optimizing daytime measurement performance in the convective PBL and were found to be $\lambda_{LoJ} = 354.36$ nm and $\lambda_{HiJ} = 353.29$ nm.

The direct calculation of the water vapor mixing ratio, w , is obtained from Raman backscattered signals through the following equation (Whiteman et al., 1992)

$$w_{H_2O}(z) = K\Delta T(z) \frac{P_{H_2O}(z)}{P_{ref}(z)} \quad (2)$$

where $P_{H_2O}(z)$ is the water vapor vibrational Raman lidar signal at wavelength λ_{H_2O} , while $P_{ref}(z)$ is a nearly temperature-independent reference signal obtained through a linear combination of the two temperature sensitive rotational Raman lidar signals $P_{LoJ}(z)$ and $P_{HiJ}(z)$ at the two nearby wavelengths λ_{LoJ} and λ_{HiJ} , K is a calibration constant (Whiteman et al., 1992; Whiteman, 2003b; Di Girolamo et al., 2018), $\Delta T(z)$ is the differential transmission term accounting for the different atmospheric transmission by molecules and aerosols at λ_{H_2O} and $\lambda_{HiJ,LoJ}$.

The vertical profile of the particle backscattering coefficient $\beta_{\lambda_0}^{par}(z)$ at $\lambda_0 = 354.7$ nm is calculated from the ratio of the elastic backscatter signal $P_{\lambda_0}(z)$ and the essentially temperature-independent reference signal $P_{ref}(z)$ through Equation 3 (Ansmann et al., 1992):

$$\beta_{\lambda_0}^{par}(z) = \beta_{\lambda_0}^{mol} \left[\frac{P_{\lambda_0}(z)}{k P_{ref}(z)} - 1 \right] \quad (3)$$

where $\beta_{\lambda_0}^{mol}$ is the backscattering coefficient at λ_0 due to Rayleigh scattering from primarily oxygen and nitrogen molecules, and k is a normalization term. The vertical profile of the particle extinction $\alpha_{\lambda_0}^{par}(z)$ can be obtained from $P_{ref}(z)$ through a modified form (Di Girolamo et al., 2006) of the equation defined by Ansmann et al. (1990).

$$\alpha_{\lambda_0}^{par}(z) = \frac{1}{2} \frac{d}{dz} \ln \left[\frac{n(z)}{P_{ref}(z) z^2} \right] - \alpha_{\lambda_0}^{mol}(z) \quad (4)$$

where $\alpha_{\lambda_0}^{mol}(z)$ is the molecular extinction coefficient at λ_0 and $n(z)$ represents the ambient gas number density.

Thus, the simulation of the performance of the candidate Raman lidar is accomplished by numerically evaluating the equations above, along with their corresponding uncertainty equations, to generate synthetic signals due to backscattered radiation at the laser wavelength (354.7 nm), vibrational Raman scattering from water vapor (407.5 nm), rotational Raman scattering from HiJ (353.29 nm) and LoJ (354.36 nm) channels. The methods used to simulate these signals will now be discussed.

2.2 Raman Water Vapor Lidar Model and Previous use, Comparison With Di Girolamo et al

The Raman lidar simulator that was used here has been used extensively for simulations of lidar measurements of water vapor from both airborne (Whiteman et al., 2001) and ground-based (Whiteman et al., 2010) platforms and is an implementation of the lidar equation, (Measures, 1984) that carries physical units through the entire simulation chain including for background skylight. The model was also recently upgraded to perform

simulations of spaceborne measurements of aerosol backscatter and extinction (Whiteman et al., 2018). To support the studies here, that model was extended further to include simulations of lidar signals from rotational Raman scattering. Prior to the work described here, comparisons were made between the water vapor and temperature profile simulations of this revised model and those in DiG2018 and excellent agreement between the models was found.

DiG2018 used four standard atmospheres (US Standard-1976, Tropical, Mid-Latitude Summer and Mid-Latitude Winter) to perform their study of spaceborne thermodynamics lidar performance. Here we make use of a 24-h orbit simulation performed by the NASA/GSFC GEOS model (Rienecker et al., 2008) to provide a large number of simulated lidar profiles under a range of geographic and climate conditions.

2.3 GEOS Dataset and 3+2 Simulations

The atmospheric profiles of water vapor, temperature, aerosols and atmospheric density that were used as input to the lidar simulator were provided by the NASA/GSFC GEOS model (Rienecker et al., 2008) for a 24-h orbit of the CALIPSO platform on 15 July 2009. A 10-s temporal resolution was used in the simulations resulting in 8,640 profiles with horizontal resolution of approximately 80 km. This is the same simulation dataset that was used in Whiteman et al., 2018 for simulating spaceborne measurements of aerosol backscatter and extinction. Skylight irradiance values were provided along with the GEOS simulations by the VLIDORT (Vector Linearized Discrete Ordinate Radiative Transfer) radiative transfer model (Spurr, 2006).

2.4 Thermodynamics Spaceborne Lidar Specifications

The spaceborne platform that is simulated here is the same as studied in DiG2018. It consists of a 4 m diameter telescope, 100 Hz laser with 2.5 J per pulse at 354.7 nm. The optical receiver uses a field of view of 25 μ rad and collects and processes signals from water vapor Raman backscatter (407.5 nm), Rayleigh-Mie backscatter (354.7 nm), HiJ and LoJ rotational Raman backscatter (353.29, 354.36 nm, respectively). The orbit considered has an altitude of 450 km and is sun-synchronous such that the solar zenith angle (SZA) always exceeds 65°. This orbit was selected to avoid the high solar background associated with brighter parts of the day. DiG2018 studied 4 standard atmosphere scenarios and concluded that the candidate thermodynamics lidar system is able to perform day- and night-time atmospheric water vapor mixing ratio and temperature measurements in cloud-free conditions with an accuracy fulfilling observational requirements for NWP. Many more details of the spaceborne lidar are contained in DiG2018, to which the authors refer the reader, and thus will not be repeated here.

Here we extend the work of DiG2018 by considering a 24-h simulation of atmospheric profiles along the CALIPSO orbit of 15 July 2009 provided by the NASA/GSFC GEOS model. Only clear sky scenarios are considered here. DiG2018 considered the

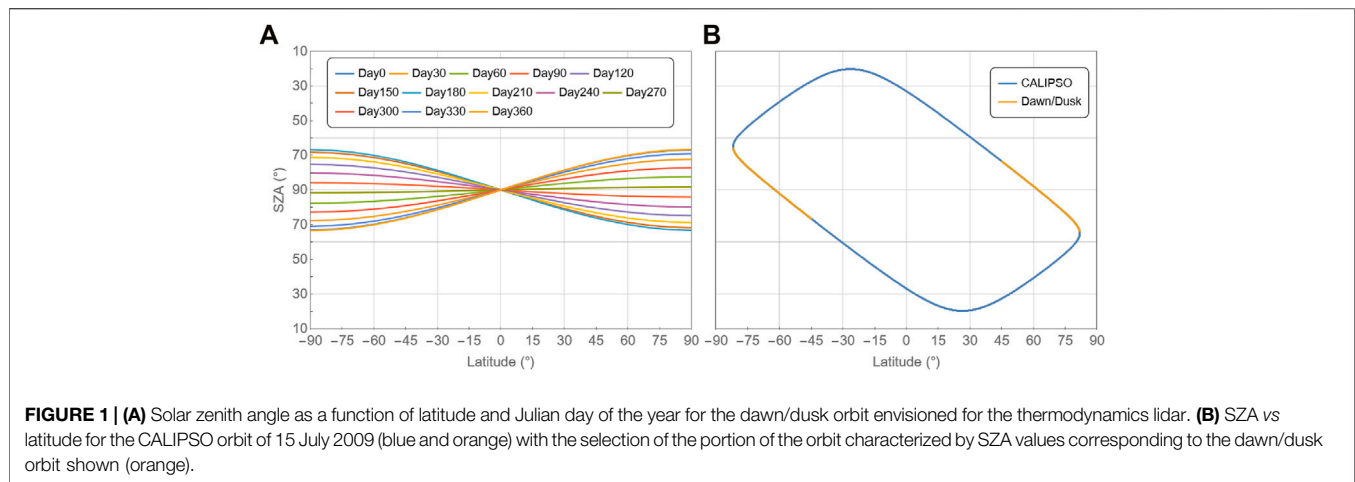


FIGURE 1 | (A) Solar zenith angle as a function of latitude and Julian day of the year for the dawn/dusk orbit envisioned for the thermodynamics lidar. **(B)** SZA vs latitude for the CALIPSO orbit of 15 July 2009 (blue and orange) with the selection of the portion of the orbit characterized by SZA values corresponding to the dawn/dusk orbit shown (orange).

TABLE 1 | OSCAR measurement metrics.

Parameter	Horizontal resolution (km)	Vertical resolution (m)	Random uncertainty
Temperature (K)	100	1,000	1 K
Specific Humidity (g/kg)	50	1,000	5%
Aerosol Backscatter Coefficient ($\text{km}^{-1} \text{sr}^{-1}$)	50	30	5%
Aerosol Extinction (km^{-1})	80	250	20%

influence of clouds and found that NWP and climate research observational requirements can be met above and below thin cirrus clouds with optical depths of 0.3. The more detailed OSSE work currently being performed will consider the full influence of clouds on forecast improvement.

2.4.1 Orbit and Skylight Considerations, Selection From the GEOS Dataset

As mentioned above, a dawn/dusk orbit for which the solar zenith angle is always greater than 65° was simulated in DiG2018. The range of SZA experienced during the dawn/dusk orbit varies by time of the year and by latitude as can be seen on the left side of **Figure 1** which is reproduced from DiG2018. The CALIPSO platform follows the A-train orbit and thus covers SZAs that are as small as $\sim 20^\circ$. To assess the performance of the thermodynamics lidar for a dawn/dusk orbit, therefore, a selection from the full 24-h CALIPSO simulation that is consistent with the dawn/dusk orbits was performed. That selection is shown on the right side of **Figure 1** with the selected {latitude, SZA} pairs being shown in yellow. This selection yielded 2,117 profiles out of the total 8,640 profiles contained in the 24-h CALIPSO orbit simulation and resulted in latitudes between ± 45.0 – 81.8° being included in the study here. Note that this sampling of the CALIPSO orbit excludes the elevated water vapor mixing ratio conditions that characterize the PBL in the lower latitudes. The effect of this selection will be discussed later. These 2,117 profiles were used as input to the lidar simulator in order to perform a statistical study of the uncertainties in the measurements of water vapor, temperature, aerosol backscatter and extinction within the PBL.

2.5 Performance Metrics

To assess the performance of the simulated thermodynamics lidar system, measurement metrics were established by considering the WMO Observing Systems Capability Analysis and Review (WMO Oscar, 2021) requirements for Global NWP and are listed in **Table 1**. OSCAR is the official repository of requirements for observation of physical variables in support of World Meteorological Programs. In the OSCAR database of atmospheric parameters, different measurement requirements are identified as “threshold”, “goal”, or “breakthrough” where “threshold” specifies the minimum requirement to be met to ensure that data are useful. As described in the OSCAR documentation, the “goal” is an ideal requirement above which further improvements are not necessary. The “breakthrough” is an intermediate level between “threshold” and “goal” which, if achieved, would result in a significant improvement for the targeted application. The breakthrough level may be considered as optimum, from a cost-benefit point of view, when planning or designing observing systems (WMO Oscar, 2021). For characterizing the performance of the spaceborne thermodynamics lidar measurements of temperature and water vapor (specific humidity), we will consider the OSCAR “breakthrough” requirements for global Numerical Weather Prediction (NWP) which are listed in **Table 1**. The OSCAR requirements for measurements of aerosol backscatter and extinction are not well-defined so we will consider metrics for those quantities that are similar to spatial and temporal resolution of airborne measurements of aerosol backscatter and extinction (Whiteman et al., 2010). The 2,117 profiles that are consistent with a dawn/dusk orbit will be assessed for their measurement

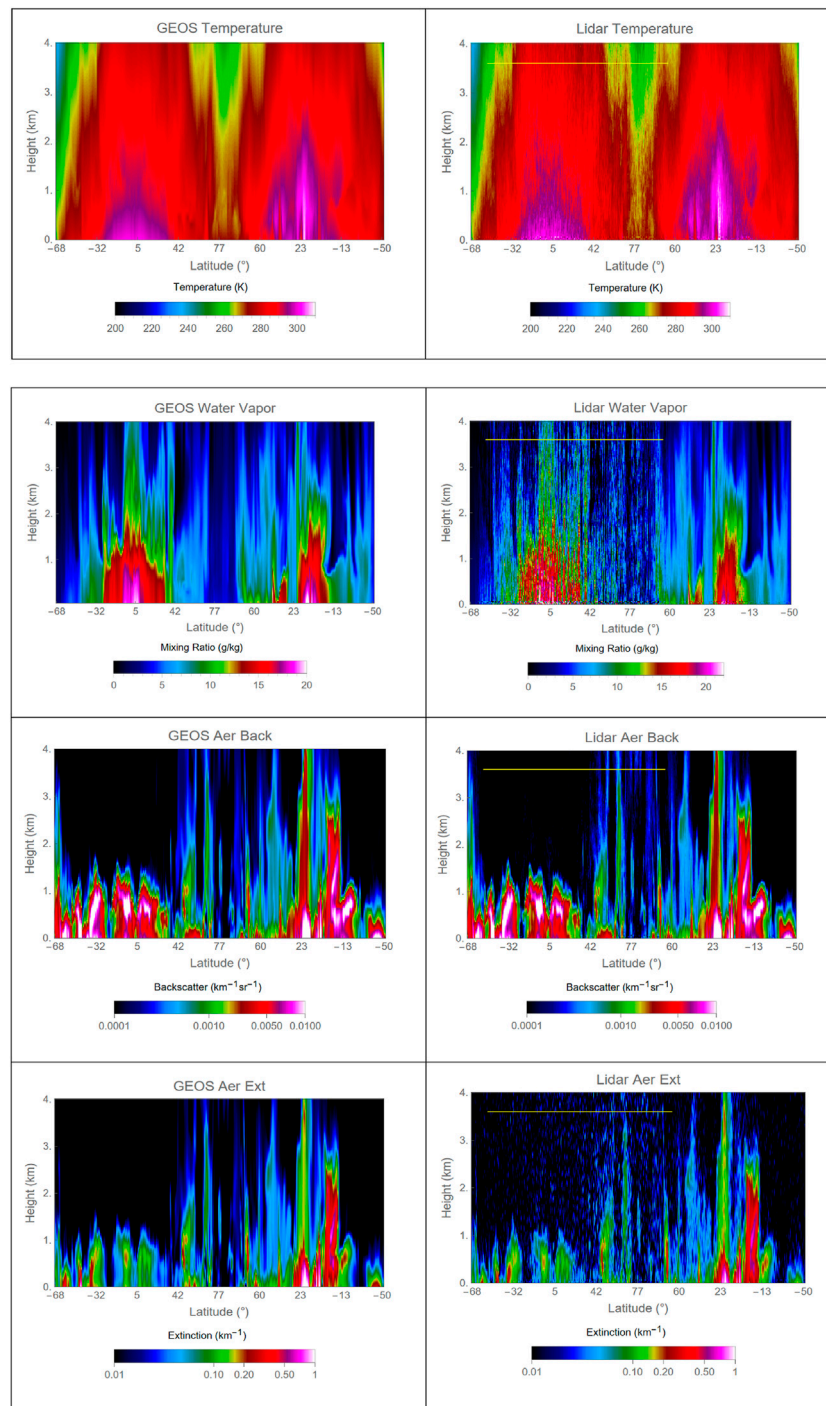
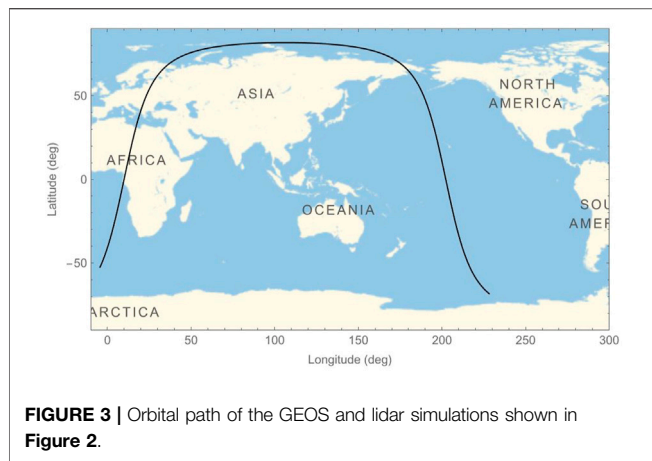


FIGURE 2 | Comparison of GEOS input and lidar simulations for approximately 1.25 h of the 24 h CALISPO orbit. The plots extend to an altitude of 4 km consistent with the focus on lidar performance within the PBL. The portion of the image where the sun is above the horizon is shown with a yellow line in the upper left of the lidar images. See text for further details.

performance based on the metrics specified in **Table 1**. Prior to presenting that statistical analysis, however, a visual illustration of simulated lidar performance within the PBL will be presented next.

3 RESULTS

To give a visual impression of what the measurements of the thermodynamics lidar system studied here would be like for the



full CALISO orbit, Figure 2 presents comparisons of approximately 1.25 h (out of the full 24-h orbit) of the GEOS input and lidar simulations of temperature, water vapor, aerosol backscatter and aerosol extinction under cloud-free conditions. On the left side of Figure 2 is shown the GEOS model inputs for temperature, water vapor mixing ratio, aerosol backscatter and extinction. On the right side of the figure are shown the corresponding lidar simulations. The orbit path that was simulated by the GEOS model is shown in Figure 3. The general fidelity of all measurements is evident from these visual displays with the comparisons of temperature and aerosol backscatter being the most impressive. There is, however, significant degradation in the water vapor measurements during full daylight conditions. The portion of the dataset with the sun above the local horizon is shown with a yellow line in the upper left of the lidar simulations. Degradation

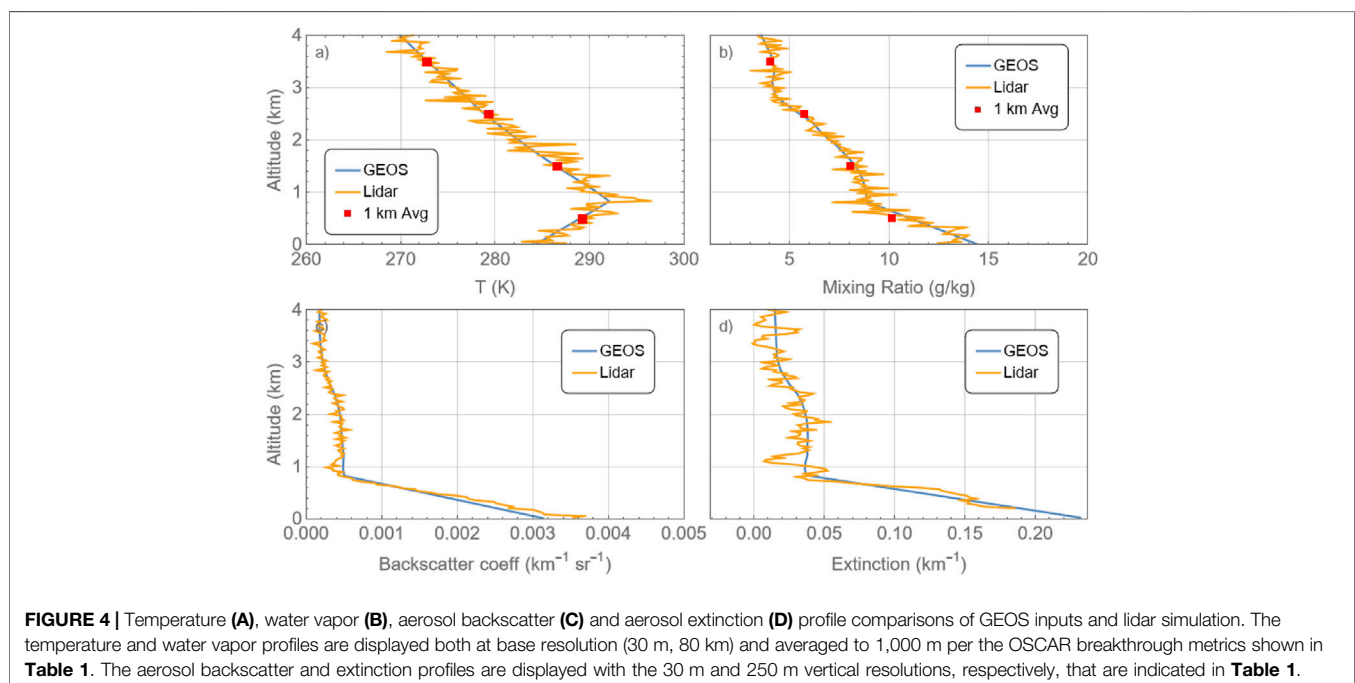
in the water vapor measurement capability during the daytime is the main motivator for the dawn/dusk orbit that was selected for the thermodynamics lidar analyzed here.

3.1 Selection From the Full CALIPSO Orbit

Now we consider example profiles from the population selected according to the dawn/dusk criteria illustrated in Figure 1 which will be used to quantify the performance of the thermodynamics lidar according to the performance metrics shown in Table 1. Figure 4 presents the temperature, water vapor mixing ratio, aerosol backscatter and extinction profiles for a location over south-central Russia when the solar zenith angle was approximately 96° . Both GEOS input and lidar simulated profiles are shown. All lidar simulations use a 10-s average. The lidar simulated temperature and water vapor profiles (top of Figure 4) are both presented with their base resolution of 30 m vertical resolution as well as averaged to 1,000 m as needed for the statistical assessment based on the OSCAR performance metrics shown in Table 1. The simulated lidar aerosol backscatter and extinction profiles (bottom) are displayed with the 30 m and 250 m vertical resolutions, respectively, that are indicated in Table 1. The lidar simulations represent well the GEOS inputs although the random fluctuations due to both skylight background and counting statistics are evident. We will now study the statistics of the 4 quantities shown in Figure 4 using the selected population that approximates the dawn/dusk orbit shown in Figure 1.

3.2 Temperature Statistics

Figure 5 presents the analysis of temperature uncertainty statistics using the uncertainty formulation shown in Equation 5 (Behrendt and Reichardt, 2000; Di Girolamo et al., 2004).



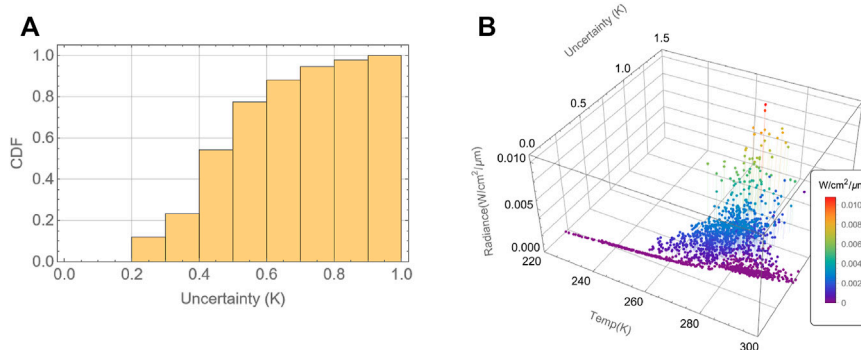


FIGURE 5 | (A) Cumulative Distribution Function for the PBL temperature uncertainty, **(B)** temperature uncertainty as a function of background radiance.

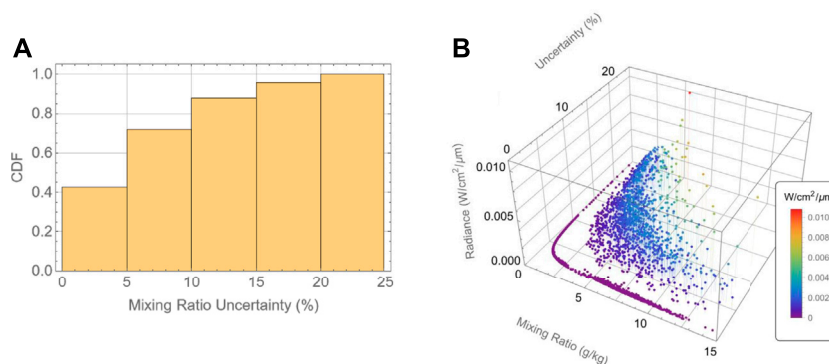


FIGURE 6 | (A) Cumulative Distribution Function for the PBL water vapor mixing ratio simulations. **(B)** water vapor mixing ratio uncertainty as a function of background radiance.

$$\Delta T(z) = \frac{\partial T(z)}{\partial Q} Q(z) \sqrt{\frac{P_{LoJ}(z) + bk_{LoJ}}{P_{LoJ}^2(z)} + \frac{P_{HiJ}(z) + bk_{HiJ}}{P_{HiJ}^2(z)}} \quad (5)$$

where all terms have been previously defined except $bk_{LoJ,HiJ}$ which represent the background signal in the *LoJ* and *HiJ* rotational Raman channels due to sky brightness and are constant as a function of range. Recall that the OSCAR breakthrough requirement from **Table 1** was 1K temperature uncertainty for measurements with 100 km horizontal and 1,000 m vertical resolution. Using those averaging parameters, **Figure 5A** presents the cumulative distribution function of temperature uncertainty for all the measurements within the PBL as identified by the GEOS model for the selected dawn/dusk profiles. Essentially 100% of the selected measurements have uncertainties less than 1K. **Figure 5B** presents the dependence of those uncertainties on both temperature and sky radiance. Under low radiance conditions (purple-colored points), the relationship of temperature and uncertainty displays a square root relationship consistent with the Poisson statistics that govern the counting process for these measurements. The presence of higher background radiance, which is related to higher solar elevation angles, increases the values of the $bk_{LoJ,HiJ}$ terms in **Equation 5** and thus the total uncertainty of the temperature measurements.

3.3 Water Vapor Statistics

Figure 6 presents an analysis of the mixing ratio uncertainty for the measurements selected that are consistent with a dawn/dusk orbit and that occurred within the PBL as identified by the GEOS model. The formulation for the water vapor mixing ratio uncertainty (Whiteman, 2003a; Whiteman, 2003b, DiG2018) that will be used is given in **Equation 6**

$$\frac{\Delta w_{H_2O}(z)}{w_{H_2O}(z)} = 100 \times \sqrt{\frac{P_{H_2O}(z) + bk_{H_2O}}{P_{H_2O}^2(z)} + \frac{P_{ref}(z) + bk_{ref}}{P_{ref}^2(z)}} \quad (6)$$

Considering the OSCAR threshold requirements of 1,000 m vertical resolution and 50 km horizontal resolution, **Figure 6A** indicates that 42% of the measurements meet the OSCAR requirement of 5% uncertainty, while 72% of the measurements have random uncertainty less than 10% and essentially all of the selected measurements have uncertainties less than 25%. These results are for a selection of cases restricted to the latitude range of 45.0–81.8°, as mentioned previously. **Figure 6B** illustrates the effect of higher background radiance levels on the mixing ratio measurements. There is a consistent increase in the uncertainty of the measurement when either the mixing ratio decreases or the radiance value increases as expected from **Equation 6**. As in the discussion relating to **Equation 5**, sun

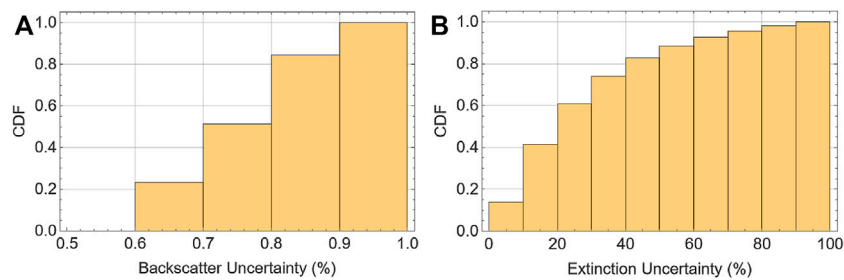


FIGURE 7 | Cumulative Distribution Function for the uncertainty in PBL aerosol backscatter coefficient (A) and aerosol extinction (B) simulations.

positions increasingly above the horizon are the main contributors to increasing background radiance values.

3.4 Aerosol Backscatter and Extinction Statistics

The equations used to assess the uncertainty of aerosol backscatter and extinction may be found in DiG2018 and are not repeated here. **Figure 7** presents the cumulative probability distributions for uncertainties in aerosol backscatter 1) and aerosol extinction 2) using the set of 2,117 selected profiles. The results indicate that, using the performance metrics listed in **Table 1** of 50 km horizontal and 30 m vertical resolution, the aerosol backscatter uncertainties always remain less than 1% easily exceeding the performance metric of 5%. This result is statistical confirmation of the high fidelity simulations shown in **Figure 2**. Using the corresponding metrics for aerosol extinction of 80 km horizontal and 250 m vertical resolution, 42% of the measurements are performed with uncertainties of 20% or less.

4 DISCUSSION

The performance of a spaceborne thermodynamics Raman lidar for measuring temperature, water vapor and aerosols is studied here using a set of metrics derived from the OSCAR database, for temperature and water vapor, as well as previous lidar performance metrics for aerosol backscatter and extinction. We use a selected set of profiles within the PBL from a simulated CALIPSO orbit performed by the NASA/GSFC GEOS model. The selection resulted in measurement simulations with solar zenith angles of 65° or greater being included thus making the sky background conditions consistent with the assumed dawn/dusk orbit of the thermodynamics orbit. However, as noted earlier, this selection of profiles included only latitudes between 45° and 81.8° thus systematically excluding the moist tropical and subtropical boundary layer environments. Note, though, that the full range of longitudes is included in the selection. The proper simulation of the thermodynamics lidar for a dawn/dusk orbit is in progress thus we only estimate here the influence of this mid-high latitude selection bias on the statistical performance of the lidar system.

To first order, we assume that the mid-high latitude selection bias has no effect on the temperature statistics since a wide range of temperatures is included in the selected profiles. We speculate that there is likely a small effect on the aerosol backscatter and extinction statistics due to the mid-high latitude selection. Some of the most polluted regimes are systematically excluded due to the current selection and these areas might be measured with improved statistics. We do not consider this effect to be large, however, thus we speculate that 50% or more of the extinction measurements could be made with uncertainties of less than 20% if the full set of latitudes had been included. The aerosol backscatter statistics will likely improve as well. However, they already well exceed the measurement metrics shown in **Table 1** indicating that the thermodynamics lidar studied here will be sensitive to even very light aerosol scattering globally.

The measurement parameter that is most affected by the mid-high latitude bias is certainly water vapor mixing ratio. The mean mixing ratio of the selected cases is less than 5 g/kg and only 5% of the selected cases have mixing ratios that exceed 10 g/kg while in the tropics mixing ratios in the boundary layer can exceed 20 g/kg. The water vapor signal received by the lidar is directly proportional to the water vapor concentration thus one can expect that measurements in the tropics could result in signals on average 3–4 times larger than the mean signals studied here. **Equation 6** shows the square root relationship of the overall uncertainty and the P_{H_2O} term complicated by the presence of the background in the water vapor channel, bk_{H_2O} . Thus, one cannot simply assume that the statistical performance will be increased under tropical conditions by $\sqrt{3}$ or $\sqrt{4}$ over the statistics shown here. Such an assessment is in progress with the proper dawn/dusk orbit. For now, we conservatively estimate that more than 50% of the water vapor cases, perhaps much more, will meet the OSCAR performance metrics shown in **Table 1**.

Summarizing the performance of the thermodynamics lidar with respect to the performance metrics shown in **Table 1** after considering the influence of the mid-high latitude bias in the case selection, we find that for the cloud-free conditions within the planetary boundary layer considered here:

- 1) Temperature: 100% the measurements will be sampled with uncertainties of less than 1 K
- 2) Water vapor mixing ratio: we estimate that more than 50% of the measurements, perhaps much more, will possess

- uncertainties less than 5% and that more than 80% of the measurements will possess uncertainties of less than 10%
- 3) Aerosol backscatter coefficient: 100% of the measurements will possess uncertainties less than 1% easily exceeding the performance metric of 5% uncertainty for this parameter
 - 4) Aerosol extinction coefficient: we estimate that more than 50% of the measurements will possess random uncertainties of less than 20%

As already stated, the rigorous assessment of the uncertainties of the thermodynamics for a full dawn/dusk orbit including the effects of clouds is in progress. However, the very positive performance metrics demonstrated here by the thermodynamics lidar system indicates that having such measurements on a global scale could strongly impact models used for weather forecasting, calibration of space-borne passive remote sensing systems and for convective scale data assimilation studies. Improvement in these areas implies that the thermodynamics lidar could thus greatly increase our understanding of and ability to predict the Earth's water and energy cycles.

DATA AVAILABILITY STATEMENT

The original contributions presented in the study are included in the article/Supplementary Material, further inquiries can be directed to the corresponding author.

REFERENCES

- Ansmann, A., Riebesell, M., and Weitkamp, C. (1990). Measurement of Atmospheric Aerosol Extinction Profiles with a Raman Lidar. *Opt. Lett.* 15, 746–748. doi:10.1364/ol.15.000746
- Ansmann, A., Wandinger, U., Riebesell, M., Weitkamp, C., and Michaelis, W. (1992). Independent Measurement of Extinction and Backscatter Profiles in Cirrus Clouds by Using a Combined Raman Elastic-Backscatter Lidar. *Appl. Opt.* 31, 7113–7131. doi:10.1364/ao.31.007113
- Behrendt, A., and Reichardt, J. (2000). Atmospheric Temperature Profiling in the Presence of Clouds with a Pure Rotational Raman Lidar by Use of an Interference-Filter-Based Polychromator. *Appl. Opt.* 39, 1372–1378. doi:10.1364/ao.39.001372
- Behrendt, A., Wulfmeyer, V., Hammann, E., Muppa, S. K., and Pal, S. (2015). Profiles of Second- to Fourth-Order Moments of Turbulent Temperature Fluctuations in the Convective Boundary Layer: First Measurements with Rotational Raman Lidar. *Atmos. Chem. Phys.* 15, 5485–5500. doi:10.5194/acp-15-5485-2015
- Bengtsson, L., Hodges, K. I., and Hagemann, S. (2004). Sensitivity of the ERA40 Reanalysis to the Observing System: Determination of the Global Atmospheric Circulation From Reduced Observations. *Tellus Ser. A: Dyn. Meteorol. Oceanogr.* 56 (5), 456–471.
- Crook, N. A. (1996). Sensitivity of Moist Convection Forced by Boundary Layer Processes to Low-Level Thermodynamic Fields. *Mon. Wea. Rev.* 124, 1767–1785. doi:10.1175/1520-0493(1996)124<1767:somcfb>2.0.co;2
- Di Girolamo, P., Behrendt, A., and Wulfmeyer, V. (2018). Space-borne Profiling of Atmospheric Thermodynamic Variables with Raman Lidar: Performance Simulations. *Opt. Express* 267, 8125–8161. doi:10.1364/oe.26.008125
- Di Girolamo, P., Marchese, R., Whiteman, D. N., and Demoz, B. B. (2004). Rotational Raman Lidar Measurements of Atmospheric Temperature in the UV. *Geophys. Res. Lett.* 31, L01106. doi:10.1029/2003GL018342
- Di Girolamo, P., Behrendt, A., and Wulfmeyer, V. (2006). Spaceborne Profiling of Atmospheric Temperature and Particle Extinction with Pure Rotational Raman

AUTHOR CONTRIBUTIONS

DW was the first author and performed the numerical simulations of the thermodynamics lidar as well as the analysis of its statistical performance. PD and NF performed simulations of profiles to compare with those generated by the model of DW in order to check and validate both models. AB consulted in all areas of the effort but particularly in the area of temperature profile measurements by lidar. VW consulted in all areas of the effort but particularly in the application of the measurements to global studies.

FUNDING

The effort reported here was supported by the NASA/GSFC Planetary Boundary Layer Science Task Group led by Dr. Joseph Santanello.

ACKNOWLEDGMENTS

Special thanks to Dr. Arlindo Da Silva, Dr. Peter Colarco and Dr. Virginie Buchard of NASA/Goddard Space Flight Center for the continuing collaboration in the use of the GEOS model for instrument simulation studies.

- Lidar and of Relative Humidity in Combination with Differential Absorption Lidar: Performance Simulations. *Appl. Opt.* 45 (11), 2474–2494.
- Dierer, S., Arpagaus, M., Seifert, A., Avgoustoglou, E., Dumitrache, R., Grazzini, F., et al. (2009). Deficiencies in Quantitative Precipitation Forecasts: Sensitivity Studies Using the COSMO Model. *Meteorol. Z.* 18, 631–645. doi:10.1127/0941-2948/2009/0420
- Ferrare, R. A., Melfi, S. H., Whiteman, D. N., Evans, K. D., and Kaufman, M. Y. J. (1998b). Raman Lidar Measurements of Aerosol Extinction and Backscattering: 2. Derivation of Aerosol Real Refractive Index, Single-Scattering Albedo, and Humidification Factor Using Raman Lidar and Aircraft Size Distribution Measurements. *J. Geophys. Res.* 103 (D16), 19673–19689. doi:10.1029/98jd01647
- Ferrare, R. A., Melfi, S. H., Whiteman, D. N., Evans, K. D., and Leifer, R. (1998a). Raman Lidar Measurements of Aerosol Extinction and Backscattering: 1. Methods and Comparisons. *J. Geophys. Res.* 103 (D16), 19663–19672. doi:10.1029/98jd01646
- Goldsmith, J. E. M., Blair, F. H., Bisson, S. E., and Turner, D. D. (1998). Turn-key Raman Lidar for Profiling Atmospheric Water Vapor, Clouds, and Aerosols. *Appl. Opt.* 37, 4979–4990. doi:10.1364/ao.37.004979
- Hammann, E., and Behrendt, A. (2015). Parametrization of Optimum Filter Passbands for Rotational Raman Temperature Measurements. *Opt. Express* 23, 30767–30782. doi:10.1364/oe.23.030767
- Kotlarski, S., Keuler, K., Christensen, O. B., Colette, A., Déqué, M., Gobiet, A., et al. (2014). Regional Climate Modeling on European Scales: A Joint Standard Evaluation of the EURO-CORDEX RCM Ensemble. *Geosci. Model. Dev.* 7, 1297–1333. doi:10.5194/gmd-7-1297-2014
- Measures, R. M. (1984). *Laser Remote Sensing Fundamentals and Applications*. Wiley-Interscience, 510.
- Melfi, S. H., and Whiteman, D. (1985). Observation of Lower-Atmospheric Moisture Structure and its Evolution Using a Raman Lidar. *Bull. Amer. Meteorol. Soc.* 66, 1288–1292. doi:10.1175/1520-0477(1985)066<1288:oolams>2.0.co;2
- NAS, National Academies of Sciences, Engineering, and Medicine (2018). *Thriving on Our Changing Planet: A Decadal Strategy for Earth Observation from Space*. Washington, DC: The National Academies Press. doi:10.17226/24938

- Raman, C. V. (1928). A Change of Wave-Length in Light Scattering. *Nature* 121 (3051), 619. doi:10.1038/121619b0
- Raman, C. V., and Krishnan, K. S. (1928). The Optical Analogue of the Compton Effect. *Nature* 121 (3053), 711. doi:10.1038/121711a0
- Rienecker, M., Suarez, M., Todling, R., Bacmeister, J., Takacs, L., Liu, H.-C., et al. (2008). The GEOS-5 Data Assimilation System—Documentation of Version 5.0.1, 5.1.0, and 5.2.0. *NASA Tech. Rep. Ser. Glob. Model. Data Assimilation* 27, 1–118.
- Sherlock, V., Hauchecorne, A., and Lenoble, J. (1999). Methodology for the Independent Calibration of Raman Backscatter Water-Vapor Lidar Systems. *Appl. Opt.* 38, 5816–5837. doi:10.1364/ao.38.005816
- Spurr, R. J. D. (2006). VLIDORT: A Linearized Pseudo-Spherical Vector Discrete Ordinate Radiative Transfer Code for Forward Model and Retrieval Studies in Multilayer Multiple Scattering media. *J. Quantitative Spectrosc. Radiative Transfer* 102 (2), 316–342. doi:10.1016/j.jqsrt.2006.05.005
- Veselovskii, I., Whiteman, D. N., Kolgotin, A., Andrews, E., and Korenskii, M. (2009). Retrieval of Aerosol Physical Properties under Varying Relative Humidity Conditions. *J. Atmos. Ocean. Tech.* 1543–1557. doi:10.1175/2009JTECHA1254.1
- Warrach-Sagi, K., Schwitalla, T., Wulfmeyer, V., and Bauer, H.-S. (2013). Evaluation of a Climate Simulation in Europe Based on the WRF-NOAH Model System: Precipitation in Germany. *Clim. Dyn.* 41, 755–774. doi:10.1007/s00382-013-1727-7
- Weitkamp, C. (2005). “Lidar, Range-Resolved Optical Remote Sensing of the Atmosphere,” in *Lidar, Range-Resolved Optical Remote Sensing of the Atmosphere*. Editor C Weitkamp (Berlin: Springer), 102. doi:10.1007/b106786
- Whiteman, D. N. (2003b). Examination of the Traditional Raman Lidar Technique. II. Evaluating the Ratios for Water Vapor and Aerosols. *Appl. Opt.* 42 (No. 15), 2593–2608. doi:10.1364/ao.42.002593
- Whiteman, D. N., Schwemmer, G., Berkoff, T., Plotkin, H., Ramos-Izquierdo, L., and Pappalardo, G. (2001). Performance Modeling of an Airborne Raman Water-Vapor Lidar. *Appl. Opt.* 40 (3), 375–390. doi:10.1364/ao.40.000375
- Whiteman, D. N. (2003a). Examination of the Traditional Raman Lidar Technique I Evaluating the Temperature-Dependent Lidar Equations. *Appl. Opt.* 42, 2571–2592. doi:10.1364/ao.42.002571
- Whiteman, D. N., Melfi, S. H., and Ferrare, R. A. (1992). Raman Lidar System for the Measurement of Water Vapor and Aerosols in the Earth’s Atmosphere. *Appl. Opt.* 31, 3068–3082. doi:10.1364/ao.31.003068
- Whiteman, D. N., Pérez-Ramírez, D., Veselovskii, I., Colarco, P., and Buchard, V. (2018). Retrievals of Aerosol Microphysics from Simulations of Spaceborne Multiwavelength Lidar Measurements. *J. Quantitative Spectrosc. Radiative Transfer* 205, 27–39. Available at: <http://www.sciencedirect.com/science/article/pii/S0022407317306398>. doi:10.1016/j.jqsrt.2017.09.009
- Whiteman, D. N., Rush, K., Rabenhorst, S., Welch, W., Cadirola, M., McIntire, G., et al. (2010). Airborne and Ground-Based Measurements Using a High-Performance Raman Lidar. *J. Atmos. Oceanic Technol.* 27, 1781–1801. doi:10.1175/2010JTECHA1391.1
- WMO Oscar (2021). OSCAR - Observing Systems Capability Analysis and Review Tool. Available at: <https://community.wmo.int/oscar> (Accessed 4 11, 2021).
- Wulfmeyer, V., Hardesty, R. M., Turner, D. D., Behrendt, A., Cadeddu, M. P., Di Girolamo, P., et al. (2015). A Review of the Remote Sensing of Lower Tropospheric Thermodynamic Profiles and its Indispensable Role for the Understanding and the Simulation of Water and Energy Cycles. *Rev. Geophys.* 53, 819–895. doi:10.1002/2014rg000476

Conflict of Interest: The authors declare that the research was conducted in the absence of any commercial or financial relationships that could be construed as a potential conflict of interest.

Publisher’s Note: All claims expressed in this article are solely those of the authors and do not necessarily represent those of their affiliated organizations, or those of the publisher, the editors and the reviewers. Any product that may be evaluated in this article, or claim that may be made by its manufacturer, is not guaranteed or endorsed by the publisher.

Copyright © 2022 Whiteman, Di Girolamo, Behrendt, Wulfmeyer and Franco. This is an open-access article distributed under the terms of the Creative Commons Attribution License (CC BY). The use, distribution or reproduction in other forums is permitted, provided the original author(s) and the copyright owner(s) are credited and that the original publication in this journal is cited, in accordance with accepted academic practice. No use, distribution or reproduction is permitted which does not comply with these terms.